Research Article Vol. 9, No. 3 / March 2021 / Photonics Research 299

PHOTONICS Research

Influence of substrate misorientation on the emission and waveguiding properties of a blue (In,Al,Ga)N laser-like structure studied by synchrotron radiation microbeam X-ray diffraction

A. Kafar,[1,2,*] A. Sakaki,[3] R. Ishii,[1] S. Stanczyk,[2,4] K. Gibasiewicz,[2] Y. Matsuda,[1] D. Schiavon,[2,4] S. Grzanka,[2,4] T. Suski,[2] P. Perlin,[2,4] M. Funato,[1] and Y. Kawakami[1]

[1]Department of Electronic Science and Engineering, Kyoto University, Kyoto 615-8510, Japan
[2]Institute of High Pressure Physics PAS, Sokolowska 29/37, 01-142 Warsaw, Poland
[3]Nichia Corporation, Anan, Tokushima 774-8601, Japan
[4]TopGaN Ltd., Sokolowska 29/37, 01-142 Warsaw, Poland
*Corresponding author: ak@unipress.waw.pl

Received 5 October 2020; accepted 24 December 2020; posted 5 January 2021 (Doc. ID 411701); published 10 February 2021

In this work, we study how an epitaxial laser-like (or superluminescent diode-like) structure is modified by intentional changes of the substrate misorientation in the range of 0.5°–2.6°. The 40 μm × 40 μm test structure with misorientation profiling was fabricated using multilevel photolithography and dry-etching. The local structural parameters were measured by synchrotron radiation microbeam X-ray diffraction, with the sampling area of below 1 μm × 1 μm. We directly obtained the relation between the misorientation and indium content in the quantum well, changing from 9% to 18%, with a high resolution (small misorientation step). We also show a good agreement of local photoluminescence emission wavelength with simulation of transition energy based on synchrotron radiation microbeam X-ray diffraction (SR-XRD) data and estimated Stokes shift. We observe that the substrate misorientation influences also the InGaN waveguide and AlGaN cladding composition. Still, we showed through simulation of the optical confinement factor of a full laser diode structure that good light guiding properties should be preserved in the whole misorientation range studied here. This proves the usefulness of misorientation modification in applications like broadband superluminescent diodes or multicolor laser arrays.

https://doi.org/10.1364/PRJ.411701

1. INTRODUCTION

Nitride light emitters have quickly evolved from first demonstrations [1–3] to commercial products [4–8] and become the part of our everyday life, and their presence is still expanding as new applications are explored [9–11]. The vast range of developments includes high optical power and efficiency [12,13], a wide choice of emission wavelength [14–17], or new functionalities [10,18,19]. One of the important aspects of a state-of-the-art device is its high crystalline quality of the structure. The morphology of the grown layers strongly depends on the epitaxial growth mode [20,21], and it is usually preferred to ensure a step-flow mode. Typically, a vicinal substrate (surface plane misoriented with respect to the atomic planes) helps in achieving a step-flow growth [22–25]. Substrate misorientation can be formed by mechanochemical polishing [26,27], which allows the formation of a smooth and defect-free surface. In the case of bulk GaN substrates, usually a moderate misorientation of 0.3°–0.6° is used. It was demonstrated that, in the case of high indium content layers grown at lowered temperatures, the increase of substrate misorientation can make a dramatic change in the layer morphology [28].

It is important to note that increasing the misorientation of the substrate can influence not only morphology. It was reported that such changes can increase the hole concentration in Mg-doped p-GaN [29] and reduce the carbon impurity incorporation [30]. On the other hand, in the case of InGaN layers, a change of In incorporation with increasing misorientation angle was revealed [31–33]. It was also demonstrated that by proper patterning of the substrate, areas of different misorientation values can be created. This enables fabrication of multicolor devices [34,35] or broadening of superluminescent diode emission spectra [36,37]. While developing the latter solution, in our previous work [38] we studied how the InGaN quantum well (QW) emission properties are modified with the changes of misorientation. We demonstrated that it is possible to obtain, during the same growth procedure, a change of the central emission wavelength of above 25 nm in the blue–violet region with a wide range of misorientation where the light intensity is rather constant.

The goal of this study is to examine in more detail how the substrate misorientation angle influences the structural parameters of the epitaxial layers (a design including layers imitating waveguide and cladding layers below the active region). Thanks to the use of synchrotron radiation microbeam X-ray diffraction (SR-XRD), we were able to study the whole structure along a misorientation profile in a range of around 0.5° to 2.8°. We directly demonstrate the relation between the misorientation and In content in the QWs as well as the photoluminescence (PL) emission wavelength and In content. Good agreement of the calculated transition energy with the experimental PL results confirms the SR-XRD result that for lowest misorientation angles the QW thickness is reduced. Interestingly, not only InGaN but also the AlGaN layer shows a modification by substrate misorientation. This is an interesting conclusion not only from the point of view of special emitters like broadband superluminescent diodes, but also standard laser diodes as it shows that the same growth procedure may give different optoelectrical parameters of the device when it is grown on different substrates.

2. FABRICATION AND EXPERIMENTAL METHODS

The epitaxial structure studied within this measurement was grown on a patterned *c*-plane bulk GaN substrate, which included areas with changing misorientation angle. The details of the fabrication procedure are presented in our previous work [38] and include multilevel photolithography and dry-etching steps that allow us to obtain 3D shapes on the substrate surface. For this study, we chose a pattern with a non-linear misorientation profile that makes it easier to study the areas with lowest and highest substrate misorientation. After the substrate was prepared, we performed metal organic vapor phase epitaxy (MOVPE) of a structure, which simulates the bottom part of a laser diode or superluminescent diode and its active region; however, the AlGaN cladding layers were thinner than in a real structure. The active region consisted of two InGaN QWs surrounded by GaN barriers. The intentional structure, optimized for growth on around 0.5° misoriented substrate, is presented in Table 1.

After the epitaxial growth, the shape of the surface of the area of interest was examined by a laser microscope, and the corresponding misorientation angle map was estimated through fitting of the experimental data. The calculation was performed based on the misorientation of the substrate measured prior to the substrate patterning. The results are presented in Fig. 1. The shape of the studied area is curved according to the design, while the topmost part shows a plateau, which is a typical feature observed in this type of samples [38]. Misorientation angle ranges from below 0.5° to around 2.8°; however, the maximal values on the diagonal of the area, which is studied by XRD, reach 2.6°.

The optical properties of the sample were studied by a microphotoluminescence (μPL) system with continuous wave excitation by a 375 nm laser diode. The scheme of the system and detailed parameters are presented in Ref. [38]. The peak emission wavelength map of the studied area is introduced in Fig. 2. We observed a large shift of emission wavelength of above 40 nm at excitation of around 0.2 kW/cm^2. Rather low excitation was used to reduce the possible blueshifting effects

Table 1. Structure of the Examined Sample[a]

Layer	Thickness (nm)	Type
GaN	32	
$In_{0.14}GaN$	2.1	QW
GaN	6.5	
$In_{0.14}GaN$	2.1	QW
GaN	6.5	
$In_{0.04}GaN:Si$	50	Waveguide
GaN:Si	10	
$Al_{0.04\to 0}GaN:Si$	100	
$Al_{0.04}GaN:Si$	100	Cladding
GaN:Si	500	
GaN substrate		

[a]Below the active region, layers imitating InGaN waveguide and AlGaN cladding of typical edge emitters are included.

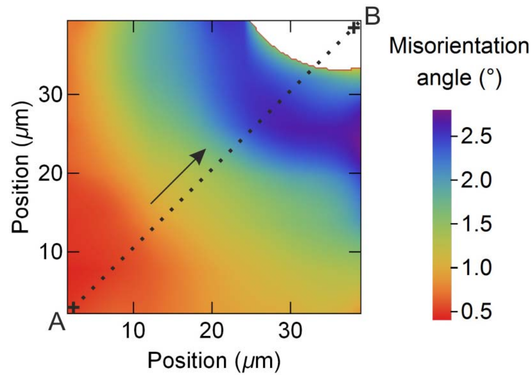

Fig. 1. 3D shape of the examined area with misorientation change and the corresponding misorientation map of this area. The dotted line presents the orientation of the synchrotron XRD scan, with the direction from A to B.

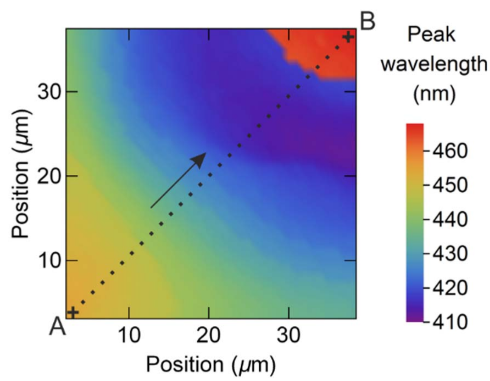

Fig. 2. Map of the peak emission wavelength of the area studied in this experiment. The map was measured with excitation power density of around 0.2 kW/cm^2. The dotted line presents the orientation of the synchrotron XRD scan, with the direction from A to B.

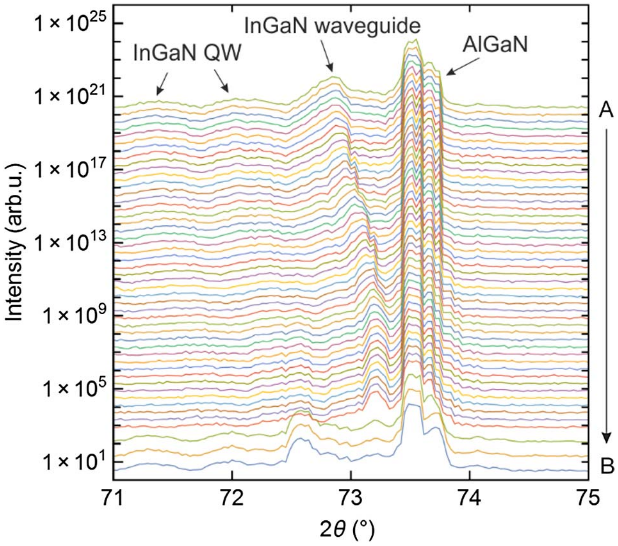

Fig. 3. Set of the XRD scans obtained along the diagonal of the test area, from point A to point B as marked in Figs. 1 and 2. A clear shift of the InGaN-related peak is observed. For clarity, the intensity scans were shifted vertically.

present at high carrier densities for the purpose of comparison with calculation presented later in this article. The distribution of the peak wavelength shows similar shapes to the misorientation map presented in Fig. 1.

The study of the structure was performed by SR-XRD using the BL16XU beamline at Super Photon ring-8 GeV (SPring-8) synchrotron. The X-ray beam of 12 keV (wavelength ≈ 0.103 nm) was shaped through a pinhole and Kirkpatrick–Baez mirrors, and irradiated onto the sample. The beam size was checked by the knife-edge method, which showed 0.41 μm vertically and 0.56 μm horizontally. The sample was mounted and positioned to enable a line scan along the diagonal of the square test area, from point A to B as marked in Figs. 1 and 2. Next, symmetric $\omega/2\theta$ measurements were performed in the vicinity of the GaN (006) reflection. Between the consecutive measurements, the sample was shifted by a 1 μm step. Figure 3 shows a comparison of the obtained XRD data. The most notable change between different scan areas is observed for the InGaN-related peak. The obtained profiles were fitted by a dynamical simulation, which is described in more detail in Ref. [39]. The averaged R factor, which is an indicator of fitting error, was changing spatially, but most positions outside of the plateau region stayed in the range between 0.029 and 0.036, with the average value of 0.032. The example average uncertainties were 0.7 nm of QW thickness estimation, 1% of In content in QWs, 0.03% of In content in the waveguide, and 0.08% of Al content in the cladding.

3. MODIFICATION OF QUANTUM WELL PROPERTIES

Next, we present in Fig. 4 the obtained In content and thickness values with respect to the position on the sample. We observe that the In content of the QWs changes from around 9% to 18%, while the layer thickness does not show a very clear

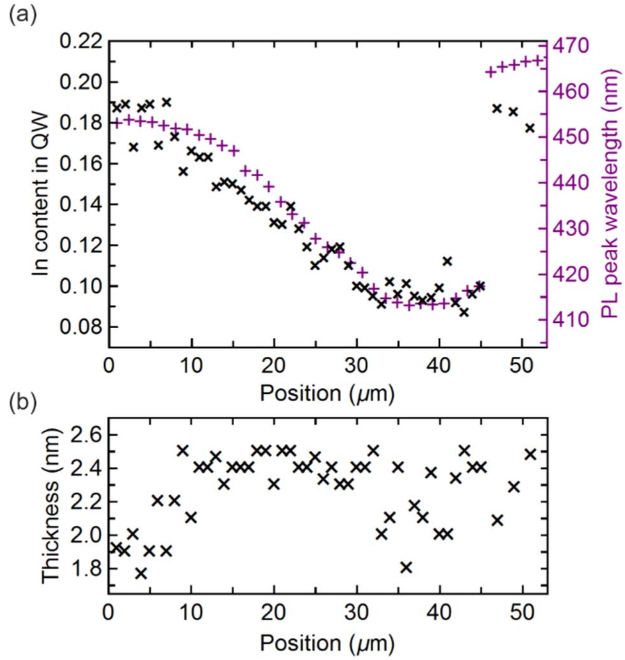

Fig. 4. Parameters of the quantum wells obtained through SR-XRD scan: (a) indium content and (b) layer thickness. The (a) plot includes also μPL peak wavelength profile based on the data presented in Fig. 2. Position 0 corresponds to point A in Figs. 1 and 2.

trend. It is possible that the QW thickness is reduced for the lowest misorientation (position below 10 μm). It needs to be emphasized that in terms of resulting emission wavelength, the thickness change leads to an opposite effect to the one related to In content change. In other words, the modification of the local PL wavelength is definitely not a result of the change of the QW thickness. Contrarily, the reduction of the QW thickness for low misorientation makes the available emission wavelength range smaller. The In content data were also compared with the data from μPL mapping (Fig. 2). The data taken from the diagonal of the μPL map were aligned with the In content profile based on the position of the plateau edge (around 46 μm). We observe that both datasets present very similar shapes. In the case of the PL data, a larger discrepancy between the plateau region and the low misorientation region (0–7 μm) can be observed. This may be a result of the presence of In content inhomogeneities, which can be the main source of emission under low excitation while the XRD measurement averages the In content value. Also, for the position range 0–7 μm in the XRD In content, we can observe two sets of contents, around 17% and 19%; however, this is probably related to scatter of the XRD fitting.

The data presented in Fig. 4 allow us to directly show the relation between the In content and PL peak wavelength. To get a better insight, we also calculated the QW transition energies based on the local thickness obtained from SR-XRD. In the calculation, we assumed single QWs with infinite barrier width and In-composition-dependent piezo and spontaneous polarizations. The obtained data also include a Stokes shift correction estimated based on a comparison of the experimental PL results and the simulation [Fig. 5(a)], and a linear fit to their

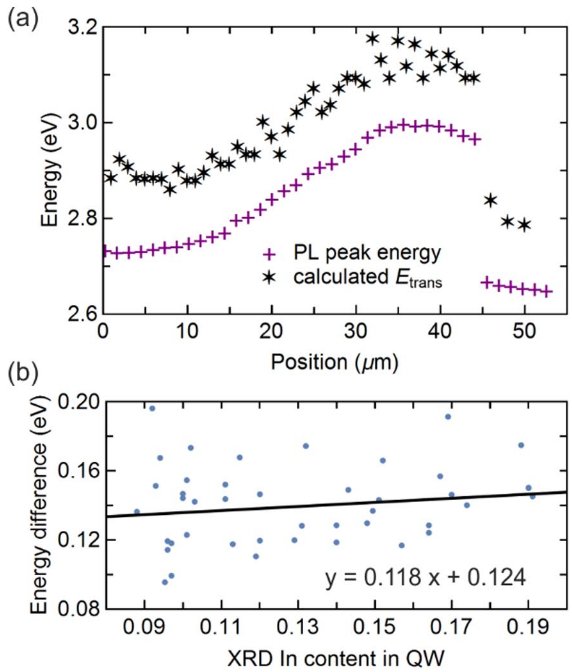

Fig. 5. Estimation of the Stokes shift of the PL emission based on comparison with the simulated transition energy. (a) The dependence of the emission energy versus position was estimated as a first-order interpolation of the experimental data and subtracted from the calculated transition energy. (b) The obtained difference was presented as a dependence on local In content and fitted with a linear function, which is used as the Stokes shift estimation.

difference [Fig. 5(b)]. It should be noted that our estimation of the Stokes shift shows very similar values to that presented by Huang *et al*. [40]. Figure 6 shows the comparison of the experimental data and the calculated values. We present both the experimental data themselves and a guide for the eye obtained by fitting the data presented in Fig. 4(a) with polynomials to reduce the noise. The presented data were chosen in a range of around 0 to 43 μm, omitting the plateau region. The obtained curve is nearly linear in the low In content (misorientation) region, but for the In contents above 13%, the dependence starts to bend downward, which suggests that there may be a change in the active region structure. One possible explanation is a decrease in the thickness of the QW, as shown in Fig. 4(b). In Fig. 6, the PL peak wavelength and the simulated emission wavelength show a very similar shape and good agreement. This suggests that the observed bend in the distribution is indeed related to the change of thickness of the QW (which is one of the input parameters of the simulation). In our previous work, we studied the QW thickness on a similar sample by transmission electron microscopy [38], which demonstrated that the QW width is most probably constant for different misorientations. However, in that case, the tested area was different—the highest measured In content was below 14.5%, and the lowest misorientation was higher than in this experiment. Within the range of position between 10 and 30 μm, the thickness observed in Fig. 4(b) can be estimated as nearly constant. Also, above 30 μm, there are many experimental points that follow the same constant trend. It is possible that for the used growth conditions there is a thickness change of the QWs when the misorientation angle is reduced below 0.6°, which corresponds to above around 15% In content.

Next, we compare the In content profile obtained from the SR-XRD with the misorientation profile of the diagonal of the map presented in Fig. 1, which is presented in Fig. 7. The data show the reduction of In content with increasing misorientation, as expected, with the fastest change for the low misorientation and a saturation at high misorientation, as shown in

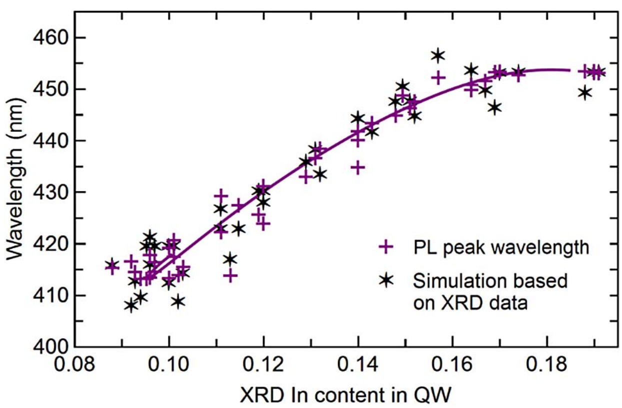

Fig. 6. Relation of the μPL peak wavelength and the In content measured by SR-XRD compared with the values obtained through simulation of transition energy for the ground states of a single QW in the presence of electric fields. The transition energy was calculated based on the local parameters obtained from XRD and corrected using the In-content-dependent Stokes shift estimated in Fig. 5. The continuous line is a guide to the eye.

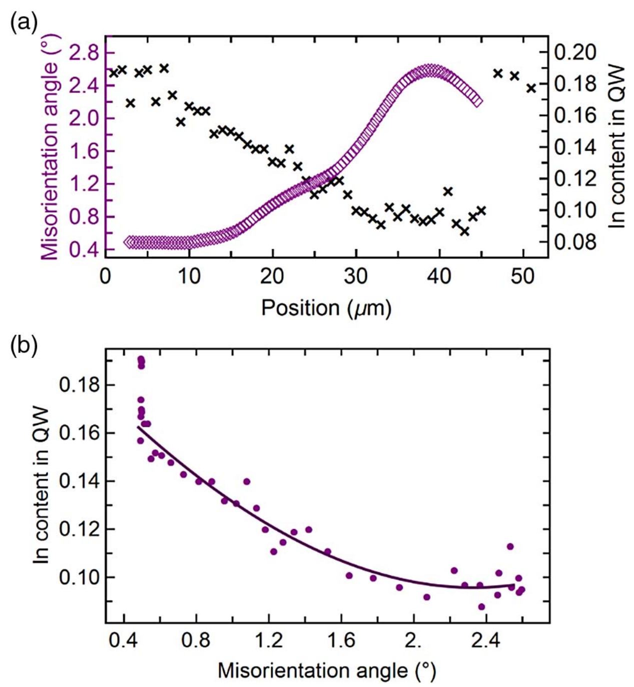

Fig. 7. Comparison of the spatial relation between the local misorientation angle and indium content in the quantum wells measured through SR-XRD: (a) as a dependence on position and (b) estimated relation of both types of values.

Fig. 7(b). This kind of shape agrees with the tendencies reported in the literature [31,35], but the exact values of the In content versus misorientation relation differ as they depend on the growth conditions. In contrast to other literature reports, in this study, we were able to obtain the dependence with a small step (high resolution in terms of the misorientation angle). The almost vertical part of the dependence is partially a consequence of the artifact related to the fitting of the misorientation map. In reality, this curve should show the further increasing of the In content with decreasing misorientation angle.

4. MODIFICATION OF WAVEGUIDE AND CLADDING PROPERTIES

The results presented to this point clearly demonstrate that the In content is closely following the change of the local misorientation of the substrate. Although such relation was already reported, our current experiment allowed us to directly compare the same positions of the sample by both PL and SR-XRD. Also, it can be safely assumed that the growth conditions (pressure, temperature, etc.) were the same during the growth of all the studied points, as the distance between the farthest studied points is below 55 μm.

The goal of our experiment utilizing the substrate misorientation change [36] is the modification of QW properties, but we also observe additional effects in other layers of the structure. Beside the InGaN QWs, our test structure includes an InGaN layer imitating the waveguide found in a full device structure. This layer has lower In content than the QWs and is grown at higher temperatures, which changes the kinetics of the In adatom incorporation during growth. But still, we can observe a very clear spatial change of the In content along the studied direction, in a range of about 2.3% to 5.1% in the main area. Surprisingly, in the plateau area the In content is much higher—around 6.8%. This distinct modification in the waveguide composition is a very important and rather negative effect from the point of view of devices (laser diodes or superluminescent diodes). The In content in the InGaN waveguide determines its refractive index, which in turn influences the waveguiding properties of the structure and its confinement factor. The change observed in Fig. 8(a) suggests that, with increasing misorientation, the waveguiding properties of the structure are worsened and it becomes more lossy. However, this effect may be partially balanced by the fact that the thickness of the layer seems to be increased in the area with smaller In content, as shown in Fig. 8(b). Also, the refractive index contrast improves at shorter wavelengths.

Even more interestingly, we observe also misorientation-related changes in the AlGaN layer imitating the cladding in a laser diode or superluminescent diode structure. In this case, the layer is much thinner than in a standard structure, but it still gives some information of the growth of AlGaN material on misoriented samples. Surprisingly, we observe that there may be a change of the Al content in the layer, similarly to what we observe in the InGaN layers—a decrease of the Al content with the increase of the misorientation. This change is less pronounced, from 3.3% to 3.9% in the main area and around 4.5% in the plateau. It should be emphasized that although

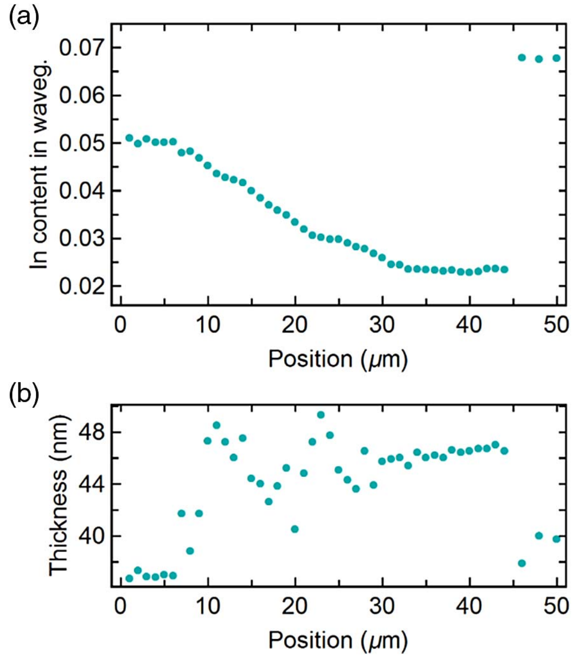

Fig. 8. Parameters of the InGaN layer obtained through SR-XRD scan: (a) indium content and (b) layer thickness. Position 0 corresponds to point A in Figs. 1 and 2.

In and Al compositions show a change in the same direction, Figs. 8(a) and 9(a)—that is, a decrease of the content for increased misorientation—the mechanism behind this change might be different. From the point of view of the atom radii, which can affect the adatom incorporation into solid, the In

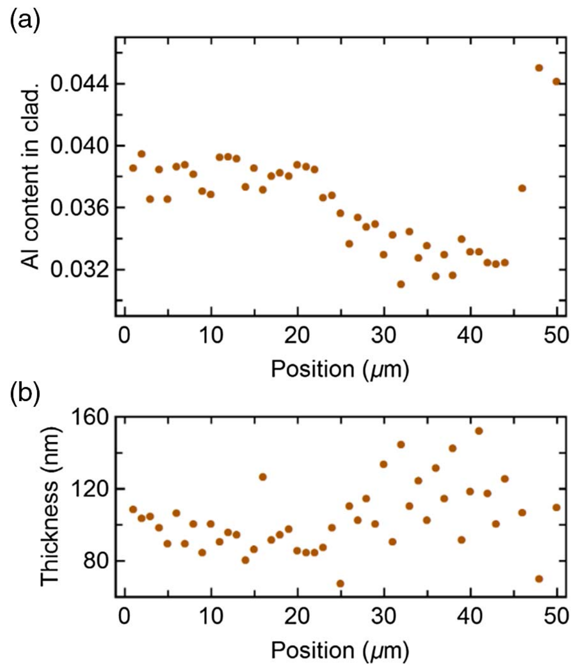

Fig. 9. Parameters of the AlGaN layer obtained through SR-XRD scan: (a) aluminum content and (b) layer thickness. Position 0 corresponds to point A in Figs. 1 and 2.

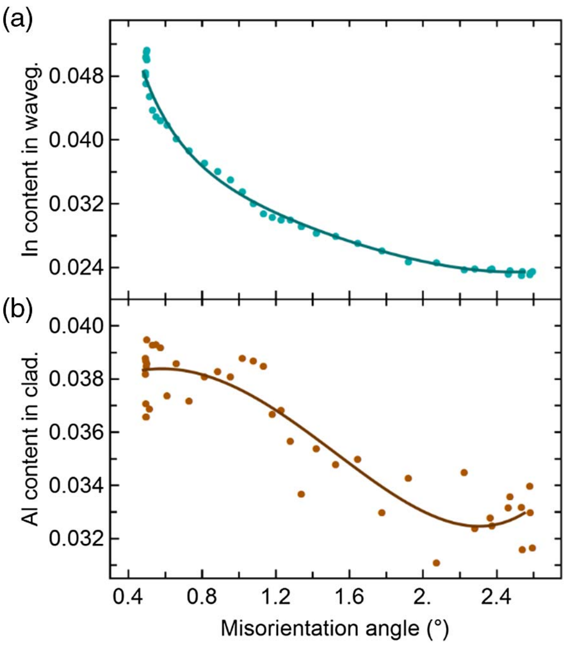

Fig. 10. Relation between the composition of layers imitating InGaN waveguide and AlGaN cladding and the local misorientation angle of the sample. The continuous lines are guides to the eye.

atoms in InGaN correspond to Ga atoms in AlGaN, which means that based on the InGaN content changes, we could expect the decrease of Ga content, and increase of Al content, in the AlGaN layer with increasing misorientation. But as it is shown in Fig. 9(a), we observe an opposite tendency. Moreover, the difference in the mechanism of composition change may be supported by the different shape of the changes—in the case of the AlGaN sample, the composition seems constant up to the position of around 20 μm, while in the case of the InGaN waveguide, the In content starts to decrease around 5 μm. It should also be noted that more effective Ga incorporation at the step edge was reported by other groups [41–45]. Although the observed change of the Al composition seems to be weak, it will contribute to the overall light guiding of the structure and may cause significant effects. It is not obvious if or how the thickness of the AlGaN layer changes with the misorientation. The obtained data show a large scatter in the area of the high misorientation in a range of even 50 nm, so it is difficult to judge.

Based on the data from SR-XRD and the measurement of the local misorientation angle (Fig. 1), we can explicitly show the relation between the compositions of the waveguiding and cladding layers and the substrate misorientation as shown in Fig. 10. In the case of the InGaN waveguide, the shape of the dependence is very similar to what is observed in Fig. 7 (b). In the case of the AlGaN layer, the modification of content is not clearly visible due to the error of the measurement, but the Al content seems to start to decrease above the misorientation of 1°. It should be noted that the misorientation map was measured after the growth in order to have a good reference for the QW parameters. As value of the misorientation may evolve during growth (shape of the surface may be modified), the distribution presented for bottom layer, AlGaN cladding, may suffer from an error of misorientation estimation.

5. SIMULATION OF A FULL DEVICE STRUCTURE

To check how the change of substrate misorientation may affect the performance of real laser diodes or superluminescent diodes, we carried out a simulation based on a standard graded index separate confinement heterostructure introduced in Ref. [46] using the SiLENSe software, for sets of layer composition and thickness data obtained through this experiment. To reduce the scatter, we first fitted the data presented in Figs. 4, 8, and 9 with low-degree polynomials. Next, we chose six positions (P1–P6) that reflected the full range of In or Al content changes of sample parameters. As our test structure, shown in Table 1, has different values of the thicknesses from a real waveguide and cladding layers, we estimated the width proportionally to the changes in the current sample assuming that the structure measured for P3 corresponds to a standard structure on a non-patterned sample. The full list of parameters that were changed during the simulation is presented in Table 2. Other parameters are assumed as presented in Ref. [46]. The wavelength of light used for the mode simulation was assumed based on the PL mapping results. The data used for this calculation are extracted from the diagonal of a map analogous to what is presented in Fig. 2, but measured at higher excitation of around 20 kW/cm^2, which is closer to the work conditions (high carrier density) of the edge-emitting devices.

Figure 11 presents the comparison of the calculated optical confinement factor (Γ) with chosen structural parameters. Most importantly, we observe that although there is a drop of Γ for the smallest and largest misorientation values, the change is moderate, and it should not prevent the device from normal operation (e.g., reaching lasing threshold in the case of laser diodes). Overall, the optical confinement factor is higher than 3.4%, which is a good value when compared with literature reports [47–50], and the maximum is reached for P3 with the value of above 3.8%. When comparing the values of Γ with other reports, it should be noted that Γ depends not only on the shape of the optical mode (related to the cladding and waveguide layers) but also on the thickness of the active area (number and thickness of the QWs). In the case of the structure simulated here, the active region consisted of three QWs. Furthermore, it seems that in the high In content region, the optical confinement factor changes may be dominated by the reduction of QW thickness, as both datasets show a similar shape. On the other hand, for the low In content region (higher misorientation), it seems that the changes may be dominated by the composition variation in the waveguide and cladding layers. It should be also noted that change of the Γ of the low In content region is reduced to some extent by the pure fact that the wavelength of propagating light is also reduced and the wavelength dependence of the refractive index influences the overall guiding of the structure. This is shown in Fig. 11(b) by the confinement factor marked by small diamonds, which was calculated for the same structural parameters as the main result but for propagating light characterized by wavelength of 439.8 nm (P3). In this case, we see a more

Table 2. Parameters Used for the Simulation of the Optical Confinement Factor in a Full Laser Structure

		Al or In Content						
	Position (μm)	**AlGaN Cladding Top**	**AlGaN EBL**	**InGaN Waveguide Top**	**InGaN QW**	**InGaN Waveguide Bottom**	**AlGaN Cladding Bottom**	**λ_{PL} (nm)**
P1	0	0.049	0.117	0.043	0.184	0.043	0.073	445.8
P2	7	0.050	0.120	0.040	0.172	0.040	0.075	446.4
P3	15	0.049	0.118	0.034	0.149	0.034	0.074	439.8
P4	23	0.047	0.112	0.026	0.122	0.026	0.070	427.4
P5	29	0.045	0.107	0.022	0.106	0.022	0.067	420.1
P6	38	0.042	0.101	0.019	0.095	0.019	0.063	412.4
		Thickness (nm)						
	(μm)	AlGaN Cladding Top	AlGaN EBL	InGaN Waveguide Top	InGaN QW	InGaN Waveguide Bottom	AlGaN Cladding Bottom	
P1	0	579	21.1	59.2	1.9	45.5	843	
P2	7	550	20.0	65.0	2.2	50.0	800	
P3	15	543	19.7	69.9	2.3	53.8	789	
P4	23	563	20.5	73.0	2.4	56.2	819	
P5	29	597	21.7	74.1	2.4	57.0	869	
P6	38	678	24.6	73.9	2.3	56.8	986	

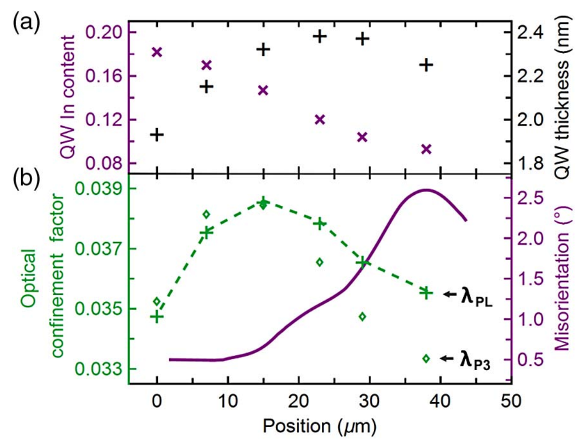

Fig. 11. Comparison of the calculated optical confinement factor Γ of the structure with other parameters as a dependence on position on the diagonal of the square pattern: (a) quantum well thickness and In content, and (b) confinement factor and local substrate misorientation. In (b), we present the optimally calculated confinement factor by crosses (based on the PL wavelength under high excitation). Additional data, depicted by diamond markers, refer to the same structural parameters as crosses but calculated for the propagating light characterized by 439.8 nm wavelength value obtained for P3.

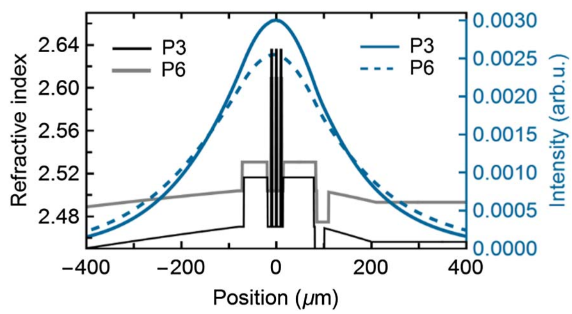

Fig. 12. Comparison of the optical mode profiles of the structure calculated based on data estimated for points P1 (position 38 μm) and P4 (position 15 μm, maximal confinement factor). The black and gray lines present the refractive index profiles for the two points.

pronounced reduction of confinement factor for lower In content region (positions above 15 μm).

In Fig. 12, we also compare the shape of the optical mode simulated for P3 and P6. The amplitude around the active layers is reduced in the case of P6, which reflects a wider spread of the mode resulting from poorer light guiding. Still, the change is not dramatic, and the shape of the mode is very similar to P3. Differences of the refractive index value are a result of both changes in the composition and different wavelength used for the calculation: 439.8 nm for P3 and 412.4 nm for P6. Both Figs. 11 and 12 suggest that although the changes of substrate misorientation angle have an impact on the whole epitaxial structure, the device work should not be seriously obstructed.

6. CONCLUSION

Within this work, we studied the properties of a nitride structure grown on an area with profiled misorientation. The experiment is based on the SR-XRD with the beam size of below 1 μm × 1 μm, allowing us to examine the sample with very high resolution. The sample included two InGaN QWs and, below, a set of layers imitating the laser diode or superluminescent diode structure: an InGaN waveguide layer and an AlGaN cladding layer. The results were compared with the data obtained from μPL mapping allowing us to show the relation between the emission wavelength and In content of the QWs in the area of changing misorientation. We observed a change of In content in a range of around 9% to 18% and proved that the shift of emission is not induced by a change of QW thickness. We were also able to reproduce the PL emission wavelength value simulating the transition energy of a QW characterized by parameters obtained through the XRD measurements. Additionally, we observed that the misorientation influences also the other layers of the structure. Both the InGaN waveguide and the AlGaN cladding seem to show a change of composition (decrease of In or Al content) with increasing misorientation. This result has important practical consequences, showing that intentionally the same epitaxial structure may change its properties significantly when it is fabricated on substrates with different misorientation. To examine this effect more explicitly, we performed simulations of full laser diode structures. We observe that although the optical confinement factor is changed when moving away from the misorientation for which the structure is optimized, the variation is rather small. This is probably thanks to both the increase of layer thickness for the regions of lowered In or Al content, as well as the wavelength dependence of the refractive index of the layers. Our results show that the usage of the substrate misorientation change does not lead to a serious structural quality deterioration and that the method is a practical approach for device fabrication.

Funding. Japan Society for the Promotion of Science (JP15H05732, JP16H02332, JP16H06426); Fundacja na rzecz Nauki Polskiej (TEAM TECH/2017-4/24).

Acknowledgment. The synchrotron radiation experiments were performed with the approval of the Japan Synchrotron Radiation Research Institute (JASRI) (Proposal Nos. 2019B5080 and 2020A5082).

Disclosures. The authors declare no conflicts of interest.

REFERENCES

1. H. Amano, M. Kito, K. Hiramatsu, and I. Akasaki, "P-type conduction in Mg-doped GaN treated with low-energy electron beam irradiation (LEEBI)," Jpn. J. Appl. Phys. **28**, L2112–L2114 (1989).
2. S. Nakamura, T. Mukai, M. Senoh, and N. Iwasa, "Thermal annealing effects on P-type Mg-doped GaN films," Jpn. J. Appl. Phys. **31**, L139–L142 (1992).
3. S. Nakamura, M. Senoh, S. Nagahama, N. Iwasa, T. Yamada, T. Matsushita, H. Kiyoku, and Y. Sugimoto, "InGaN-based multi-quantum-well-structure laser diodes," Jpn. J. Appl. Phys. **35**, L74–L76 (1996).
4. Y. Narukawa, M. Ichikawa, D. Sanga, M. Sano, and T. Mukai, "White light emitting diodes with super-high luminous efficacy," J. Phys. D **43**, 354002 (2010).
5. T. Taki and M. Strassburg, "Review—visible LEDs: more than efficient light," ECS J. Solid State Sci. Technol. **9**, 015017 (2020).
6. Y. Nakatsu, Y. Nagao, K. Kozuru, T. Hirao, E. Okahisa, S. Masui, T. Yanamoto, and S. Nagahama, "High-efficiency blue and green laser diodes for laser displays," Proc. SPIE **10918**, 109181D (2019).
7. U. Strauß, T. Hager, G. Brüderl, T. Wurm, A. Somers, C. Eichler, C. Vierheilig, A. Löffler, J. Ristic, and A. Avramescu, "Recent advances in c-plane GaN visible lasers," Proc. SPIE **8986**, 89861L (2014).
8. M. Kawaguchi, O. Imafuji, S. Nozaki, H. Hagino, K. Nakamura, S. Takigawa, T. Katayama, and T. Tanaka, "Record-breaking high-power InGaN-based laser-diodes using novel thick-waveguide structure," in *International Semiconductor Laser Conference (ISLC)* (2016), pp. 1–2.
9. P. M. Pattison, J. Y. Tsao, and M. R. Krames, "Light-emitting diode technology status and directions: opportunities for horticultural lighting," Acta Hortic. **1134**, 413–426 (2016).
10. C. Lee, C. Shen, C. Cozzan, R. M. Farrell, J. S. Speck, S. Nakamura, B. S. Ooi, and S. P. DenBaars, "Gigabit-per-second white light-based visible light communication using near-ultraviolet laser diode and red-, green-, and blue-emitting phosphors," Opt. Express **25**, 17480–17487 (2017).
11. A. D. Ludlow, M. M. Boyd, J. Ye, E. Peik, and P. O. Schmidt, "Optical atomic clocks," Rev. Mod. Phys. **87**, 637–701 (2015).
12. H. König, M. Ali, W. Bergbauer, J. Brückner, G. Bruederl, C. Eichler, S. Gerhard, U. Heine, A. Lell, L. Nähle, M. Peter, J. Ristic, G. Rossbach, A. Somers, B. Stojetz, S. Tautz, J. Wagner, T. Wurm, U. Strauss, M. Baumann, A. Balck, and V. Krause, "Visible GaN laser diodes: from lowest thresholds to highest power levels," Proc. SPIE **10939**, 109390C (2019).
13. L. Y. Kuritzky, C. Weisbuch, and J. S. Speck, "Prospects for 100% wall-plug efficient III-nitride LEDs," Opt. Express **26**, 16600–16608 (2018).
14. S. M. Islam, K. Lee, J. Verma, V. Protasenko, S. Rouvimov, S. Bharadwaj, H. Xing, and D. Jena, "MBE-grown 232–270 nm deep-UV LEDs using monolayer thin binary GaN/AlN quantum heterostructures," Appl. Phys. Lett. **110**, 041108 (2017).
15. Z. Zhang, M. Kushimoto, T. Sakai, N. Sugiyama, L. J. Schowalter, C. Sasaoka, and H. Amano, "A 271.8 nm deep-ultraviolet laser diode for room temperature operation," Appl. Phys. Express **12**, 124003 (2019).
16. Z. Bi, T. Lu, J. Colvin, E. Sjögren, N. Vainorius, A. Gustafsson, J. Johansson, R. Timm, F. Lenrick, R. Wallenberg, B. Monemar, and L. Samuelson, "Realization of ultrahigh quality InGaN platelets to be used as relaxed templates for red micro-LEDs," ACS Appl. Mater. Interfaces **12**, 17845–17851 (2020).
17. K. H. Li, Y. F. Cheung, W. Jin, W. Y. Fu, A. T. L. Lee, S. C. Tan, S. Y. Hui, and H. W. Choi, "InGaN RGB light-emitting diodes with monolithically integrated photodetectors for stabilizing color chromaticity," IEEE Trans. Ind. Electron. **67**, 5154–5160 (2020).
18. M. Wei, K. Houser, A. David, and M. Krames, "Colour gamut size and shape influence colour preference," Lighting Res. Technol. **49**, 992–1014 (2017).
19. T. J. Slight, S. Stanczyk, S. Watson, A. Yadav, S. Grzanka, E. Rafailov, P. Perlin, S. P. Najda, M. Leszczyński, S. Gwyn, and A. E. Kelly, "Continuous-wave operation of (Al,In)GaN distributed-feedback laser diodes with high-order notched gratings," Appl. Phys. Express **11**, 112701 (2018).
20. G. B. Stephenson, J. A. Eastman, C. Thompson, O. Auciello, L. J. Thompson, A. Munkholm, P. Fini, S. P. DenBaars, and J. S. Speck, "Observation of growth modes during metal-organic chemical vapor deposition of GaN," Appl. Phys. Lett. **74**, 3326–3328 (1999).
21. R. A. Oliver, M. J. Kappers, C. J. Humphreys, and G. A. D. Briggs, "Growth modes in heteroepitaxy of InGaN on GaN," J. Appl. Phys. **97**, 013707 (2005).
22. P. A. Grudowski, A. L. Holmes, C. J. Eiting, and R. D. Dupuis, "The effect of substrate misorientation on the photoluminescence properties of GaN grown on sapphire by metalorganic chemical vapor deposition," Appl. Phys. Lett. **69**, 3626–3628 (1996).
23. T. Yuasa, Y. Ueta, Y. Tsuda, A. Ogawa, M. Taneya, and K. Takao, "Effect of slight misorientation of sapphire substrate on metalorganic chemical vapor deposition growth of GaN," Jpn. J. Appl. Phys. **38**, L703–L705 (1999).
24. D. Lu, D. I. Florescu, D. S. Lee, V. Merai, A. Parekh, J. C. Ramer, S. P. Guo, and E. Armour, "Advanced characterization studies of sapphire substrate misorientation effects on GaN-based LED device development," Phys. Status Solidi A **200**, 71–74 (2003).
25. C. Sasaoka, F. Miyasaka, T. Koi, M. Kobayashi, Y. Murase, Y. Ando, and A. A. Yamaguchi, "Surface morphologies and optical properties of Si doped InGaN multi-quantum-well grown on vicinal bulk GaN(0001) substrates," Jpn. J. Appl. Phys. **52**, 115601 (2013).
26. J. L. Weyher, S. Müller, I. Grzegory, and S. Porowski, "Chemical polishing of bulk and epitaxial GaN," J. Cryst. Growth **182**, 17–22 (1997).
27. P. R. Tavernier, T. Margalith, L. A. Coldren, S. P. DenBaars, and D. R. Clarke, "Chemical mechanical polishing of gallium nitride," Electrochem. Solid-State Lett. **5**, G61 (2002).
28. A. Tian, J. Liu, L. Zhang, L. Jiang, M. Ikeda, S. Zhang, D. Li, P. Wen, Y. Cheng, X. Fan, and H. Yang, "Significant increase of quantum

efficiency of green InGaN quantum well by realizing step-flow growth," Appl. Phys. Lett. **111**, 112102 (2017).
29. T. Suski, E. Litwin-Staszewska, R. Piotrzkowski, R. Czernecki, M. Krysko, S. Grzanka, G. Nowak, G. Franssen, L. H. Dmowski, M. Leszczynski, P. Perlin, B. Łucznik, I. Grzegory, and R. Jakieła, "Substrate misorientation induced strong increase in the hole concentration in Mg doped GaN grown by metalorganic vapor phase epitaxy," Appl. Phys. Lett. **93**, 172117 (2008).
30. L. Jiang, J. Liu, A. Tian, X. Ren, S. Huang, W. Zhou, L. Zhang, D. Li, S. Zhang, M. Ikeda, and H. Yang, "Influence of substrate misorientation on carbon impurity incorporation and electrical properties of p-GaN grown by metalorganic chemical vapor deposition," Appl. Phys. Express **12**, 055503 (2019).
31. M. Sarzynski, M. Leszczynski, M. Krysko, J. Z. Domagala, R. Czernecki, and T. Suski, "Influence of GaN substrate off-cut on properties of InGaN and AlGaN layers," Cryst. Res. Technol. **47**, 321–328 (2012).
32. S. Keller, C. S. Suh, N. A. Fichtenbaum, M. Furukawa, R. Chu, Z. Chen, K. Vijayraghavan, S. Rajan, S. P. DenBaars, J. S. Speck, and U. K. Mishra, "Influence of the substrate misorientation on the properties of N-polar InGaN/GaN and AlGaN/GaN heterostructures," J. Appl. Phys. **104**, 093510 (2008).
33. K. Shojiki, T. Hanada, T. Shimada, Y. Liu, R. Katayama, and T. Matsuoka, "Tilted domain and indium content of InGaN layer on *m*-plane GaN substrate grown by metalorganic vapor phase epitaxy," Jpn. J. Appl. Phys. **51**, 04DH01 (2012).
34. M. Sarzyński, T. Suski, G. Staszczak, A. Khachapuridze, J. Z. Domagała, R. Czernecki, J. Plesiewicz, J. Pawłowska, S. P. Najda, M. Boćkowski, P. Perlin, and M. Leszczyński, "Lateral control of indium content and wavelength of III–nitride diode lasers by means of GaN substrate patterning," Appl. Phys. Express **5**, 021001 (2012).
35. P. A. Dróżdż, M. Sarzyński, J. Z. Domagała, E. Grzanka, S. Grzanka, R. Czernecki, Ł. Marona, K. P. Korona, and T. Suski, "Monolithic cyan–violet InGaN/GaN LED array," Phys. Status Solidi A **214**, 1600815 (2017).
36. A. Kafar, S. Stanczyk, M. Sarzynski, S. Grzanka, J. Goss, G. Targowski, A. Nowakowska-Siwinska, T. Suski, and P. Perlin, "Nitride superluminescent diodes with broadened emission spectrum fabricated using laterally patterned substrate," Opt. Express **24**, 9673–9682 (2016).
37. A. Kafar, S. Stanczyk, M. Sarzynski, S. Grzanka, J. Goss, I. Makarowa, A. Nowakowska-Siwinska, T. Suski, and P. Perlin, "InAlGaN superluminescent diodes fabricated on patterned substrates: an alternative semiconductor broadband emitter," Photon. Res. **5**, A30–A34 (2017).
38. A. Kafar, R. Ishii, K. Gibasiewicz, Y. Matsuda, S. Stanczyk, D. Schiavon, S. Grzanka, M. Tano, A. Sakaki, T. Suski, P. Perlin, M. Funato, and Y. Kawakami, "Above 25 nm emission wavelength shift in blue-violet InGaN quantum wells induced by GaN substrate misorientation profiling: towards broad-band superluminescent diodes," Opt. Express **28**, 22524–22539 (2020).
39. A. Sakaki, M. Funato, T. Kawamura, J. Araki, and Y. Kawakami, "Synchrotron radiation microbeam X-ray diffraction for nondestructive assessments of local structural properties of faceted InGaN/GaN quantum wells," Appl. Phys. Express **11**, 031001 (2018).
40. Y. H. Huang, C. L. Cheng, T. T. Chen, Y. F. Chen, and K. T. Tsen, "Studies of Stokes shift in $In_xGa_{1-x}N$ alloys," J. Appl. Phys. **101**, 103521 (2007).
41. M. Hayakawa, Y. Hayashi, S. Ichikawa, M. Funato, and Y. Kawakami, "Enhanced radiative recombination probability in AlGaN quantum wires on (0001) vicinal surface," Proc. SPIE **9926**, 99260S (2016).
42. I. Bryan, Z. Bryan, S. Mita, A. Rice, L. Hussey, C. Shelton, J. Tweedie, J.-P. Maria, R. Collazo, and Z. Sitar, "The role of surface kinetics on composition and quality of AlGaN," J. Cryst. Growth **451**, 65–71 (2016).
43. I. O. Mayboroda, A. A. Knizhnik, Yu. V. Grishchenko, I. S. Ezubchenko, M. L. Zanaveskin, O. A. Kondratev, M. Yu. Presniakov, B. V. Potapkin, and V. A. Ilyin, "Growth of AlGaN under the conditions of significant gallium evaporation: phase separation and enhanced lateral growth," J. Appl. Phys. **122**, 105305 (2017).
44. U. Zeimer, V. Kueller, A. Knauer, A. Mogilatenko, M. Weyers, and M. Kneissl, "High quality AlGaN grown on ELO AlN/sapphire templates," J. Cryst. Growth **377**, 32–36 (2013).
45. K. Kataoka, T. Narita, K. Horibuchi, H. Makino, K. Nagata, and Y. Saito, "Formation mechanism and suppression of Ga-rich streaks at macro-step edges in the growth of AlGaN on an AlN/sapphire-template," J. Cryst. Growth **534**, 125475 (2020).
46. S. Stanczyk, A. Kafar, S. Grzanka, M. Sarzynski, R. Mroczynski, S. Najda, T. Suski, and P. Perlin, "450 nm (Al,In)GaN optical amplifier with double 'j-shape' waveguide for master oscillator power amplifier systems," Opt. Express **26**, 7351–7357 (2018).
47. L. Q. Zhang, D. S. Jiang, J. J. Zhu, D. G. Zhao, Z. S. Liu, S. M. Zhang, and H. Yang, "Confinement factor and absorption loss of AlInGaN based laser diodes emitting from ultraviolet to green," J. Appl. Phys. **105**, 023104 (2009).
48. W. G. Scheibenzuber, U. T. Schwarz, L. Sulmoni, J. Dorsaz, J.-F. Carlin, and N. Grandjean, "Recombination coefficients of GaN-based laser diodes," J. Appl. Phys. **109**, 093106 (2011).
49. L. Redaelli, H. Wenzel, J. Piprek, T. Weig, S. Einfeldt, M. Martens, G. Lukens, U. T. Schwarz, and M. Kneissl, "Index-antiguiding in narrow-ridge GaN-based laser diodes investigated by measurements of the current-dependent gain and index spectra and by self-consistent simulation," IEEE J. Quantum Electron. **51**, 2000506 (2015).
50. J. Yang, D. G. Zhao, D. S. Jiang, X. Li, F. Liang, P. Chen, J. J. Zhu, Z. S. Liu, S. T. Liu, L. Q. Zhang, and M. Li, "Performance of InGaN based green laser diodes improved by using an asymmetric InGaN/InGaN multi-quantum well active region," Opt. Express **25**, 9595–9602 (2017).